2020 IEEE/RSJ International Conference on Intelligent Robots and Systems (IROS)
October 25-29, 2020, Las Vegas, NV, USA (Virtual)

Dual-Arm Control for Enhanced Magnetic Manipulation

Giovanni Pittiglio[1], James H. Chandler[1], Michiel Richter[2], Venkatasubramanian K. Venkiteswaran[2], Sarthak Misra[2], Pietro Valdastri[1]

***Abstract*— Magnetically actuated soft robots have recently been identified for application in medicine, due to their potential to perform minimally invasive exploration of human cavities. Magnetic solutions permit further miniaturization when compared to other actuation techniques, without loss in functionalities. Our long-term goal is to propose a novel actuation method for magnetically actuated soft robots, based on dual-arm collaborative magnetic manipulation. A fundamental step in this direction is to show that this actuation method is capable of controlling up to 8 coincident, independent Degrees of Freedom (DOFs). In present paper, we prove this concept by measuring the independent wrench components on a second pair of static permanent magnets, by means of a high resolution 6-axis load cell. The experiments show dominant activation of the desired DOFs, with mean cross-activation error of the undesired DOFs ranging from 2% to 10%.**

***Index Terms*— Medical Robots and Systems, Dual Arm Manipulation, Force Control.**

I. Introduction

The last few decades have seen a significant growth of *minimally invasive procedures for diagnosis and treatment*. This generally equates to reduced pain, morbidity and recovery time. However, the application of minimally invasive techniques poses several challenges which have led to focused investigation of multi-Degrees of Freedom (DOFs), flexible structures: *continuum robots* [1], [2], [3]. These manipulators are characterised by several DOFs and low stiffness, which facilitates the safe exploration of tortuous environments.

Continuum robots have proven effective in several scenarios, and many diverse actuation mechanisms have been proposed, for example: *concentric tubes* [4]; *(multi-)backbone-based* designs [5], [6]; *tendon driven* structures [7], [8], [9]; and soft *pneumatic* [10]; and *hydraulic* [11] implementations, among others. In general, these approaches comply with the requirements of minimally invasive procedures. However, they require physical coupling between the actuation unit and the continuum structure. This typically nessecitates an increase in their size when more DOFs are required. For this reason, *magnetic actuation* has been recently proposed for actuating continuum robots [12], [13], as an improvement to controlling single magnet-based structures [14], [15], [16]. Moreover, this concept has been further investigated also for application to soft magnetized platforms [17].

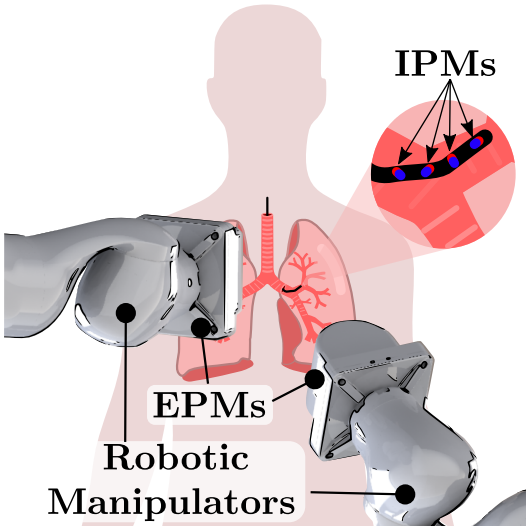

Fig. 1. Example of application of multi-DOFs magnetic manipulation in endoscopy: bronchoscopy.

In the case of magnetically actuated robots, reducing the volume of magnetic material, as necessary for miniaturization, results in a loss of magnetic wrench for a given field. However, this can be directly compensated through dimensioning of the actuation system. Specifically, more force/torque can be achieved by using more powerful actuation platforms, without a direct increase in the robot's dimensions, e.g. [18]. Several diverse actuation systems have been proposed for magnetic actuation, which can be subdivided into *coil-based* [18], [19], [20], [15], [21], [12], *rotating permanent magnets* [22], *robotically actuated coils* [23] and *robotically actuated permanent magnets* [24], [14]. The main limitation of the former two is the limited workspace and poor scalability, while their robotically actuated counterpart [24], [23] have, generally, larger manipulability workspace with only limitation to the specific robot's capabilities. However, using permanent magnets as alternative to coils

Research reported in this article was supported by the Royal Society, by the Engineering and Physical Sciences Research Council (EPSRC) under grant number EP/R045291/1, and by the European Research Council (ERC) under the European Unions Horizon 2020 research and innovation programme (grant agreement No 818045). Any opinions, findings and conclusions, or recommendations expressed in this article are those of the authors and do not necessarily reflect the views of the Royal Society, EPSRC, or the ERC.

[1]G. Pittiglio, J. H. Chandler, P. Valdastri are affiliated with the STORM Lab, School of Electronic and Electrical Engineering, University of Leeds, Leeds, UK. {g.pittiglio, j.h.chandler, p.valdastri}@leeds.ac.uk.

[2]M. Richter, V. K. Venkiteswaran and S. Misra are affiliated with the Surgical Robotics Laboratory, Department of Biomechanical Engineering, University of Twente 7500 AE, Enschede, The Netherlands. {m.richter@student., v.kalpathyvenkiteswaran@, s.misra@}utwente.nl

S. Misra is also affiliated with the Department of Biomedical Engineering, University of Groningen and University Medical Centre Groningen, 9713 GZ Groningen, The Netherlands.

facilitates energy reduction and possible electromagnetic interference.

In [21], the authors show that a set of 8 coils is able to manipulate 8 independent DOFs. This is the maximum number of DOFs that can be physically controlled in the same point of a magnetic workspace. Here, we aim to prove that same capabilities can be achieved with a minimal number of magnetic sources, i.e. 2, and that we can employ permanent magnets instead of coils. These two fundamental points facilitate cost reduction and enlarge the (magnetic) manipulability workspace, which is fundamental in the application to medical robotics. However, the proposed approach could also be applied to robotically actuated coil systems [23].

Recently, robotically manipulated single External Permanent Magnet (EPM)-based approaches have been shown to be effective in overcoming the challenges related to magnetic manipulation via non-homogeneous magnetic fields [25], [24]. Specifically, the difficulties in handling non-linear relationship between actuation variables (EPM-Internal Permanent Magnet (IPM) relative pose) and resulting wrench. However, the use of a single magnetic source limits the number of controllable DOFs to 5, given the dipole symmetries [26]. In this paper, we investigate the minimum number of magnetic sources able to achieve maximum manipulability (8 DOFs) in a single point of the workspace: 2 robotically manipulated EPMs.

The problem of magnetic manipulation with robotically actuated magnetic sources is introduced in Section II and, on the basis of this definition, we formulate the concept of *magnetic manipulability* in Section III. Possible independent poses of the EPMs are analysed in Section IV and experimentally validated in Section V. We report our main conclusions and future directions in Section VI.

II. Problem Definition

In the present section, we discuss multi-DOFs manipulation, based on magnetic wrench control [25], [24]. In particular, we consider that we can manipulate N independent IPMs, by robotically controlling the pose of M EPMs, independently.

Consider the relative position between the i-th EPM (p_{E_i}) and the j-th IPM (p_{I_j}), $p_{ij} = p_{E_i} - p_{I_j} \in \mathbb{R}^3$ and between the j-th and the k-th IPMs $d_{jk} = p_{I_k} - p_{I_j} \in \mathbb{R}^3$, and introduce the relative *magnetic wrench* [24]

$$
\begin{aligned}
w_{ij} &= \begin{pmatrix} f_{ij} \\ \tau_{ij} \end{pmatrix} \qquad (1)\\
&= \begin{pmatrix} \frac{3C_{ij}}{||p_{ij}||^4}(\hat{m}_{E_i}\hat{m}_{I_j}^T + \hat{m}_{I_j}\hat{m}_{E_i}^T + (\hat{m}_{I_j}^T Z_{ij}\hat{m}_{E_i})I)\hat{p}_{ij} \\ \frac{C_{ij}}{||p_{ij}||^3}\hat{m}_{I_j} \times D_{ij}\hat{m}_{E_i} \end{pmatrix} \\
&\quad + \sum_{k=1}^{N} \\
&\quad \begin{pmatrix} \frac{3\mathcal{C}_{jk}}{||d_{jk}||^4}(\hat{m}_{I_k}\hat{m}_{I_j}^T + \hat{m}_{I_j}\hat{m}_{I_k}^T + (\hat{m}_{I_j}^T \mathcal{Z}_{jk}\hat{m}_{I_k})I)\hat{d}_{jk} \\ \frac{\mathcal{C}_{jk}}{||d_{jk}||^3}\hat{m}_{I_j} \times \mathcal{D}_{jk}\hat{m}_{I_k} \end{pmatrix}
\end{aligned}
$$

where $C_{ij} = \frac{\mu_0||m_{I_j}||\ ||m_{E_i}||}{4\pi}$, $\mathcal{C}_{jk} = \frac{\mu_0||m_{I_j}||\ ||m_{I_k}||}{4\pi}$, with $m_{I_j}, m_{I_k}, m_{E_i} \in \mathbb{R}^3$ *magnetic moments* of the respective IPMs and EPM; $\mu_0 = 4\pi 10^{-7}\frac{N}{A^2}$ permeability of vacuum, $Z_{ij} = I - 5\hat{p}_{ij}\hat{p}_{ij}^T$, $D_{ij} = 3\hat{p}_{ij}\hat{p}_{ij}^T - I$, $\mathcal{Z}_{ik} = I - 5\hat{d}_{jk}\hat{d}_{jk}^T$ and $\mathcal{D}_{ik} = 3\hat{d}_{jk}\hat{d}_{jk}^T - I$. We refer to $I \in \mathbb{R}^{3\times 3}$ as the *identity matrix*, $||\cdot||$ as the *Euclidean norm* and $\hat{\cdot} = \frac{\cdot}{||\cdot||}$. Here, f_{ij} and τ_{ij} are the force and torque, respectively. The wrench in (1) is found by appling the *superposition principle* under the assumption that the IPMs and EPMs involved can be modeled as *dipoles*, i.e. when they are *far enough* from each other, relative to their size [27]; this is a common approach in magnetic manipulation [26].

Compared to the case of coils [21], we can notice that (1) is highly nonlinear with respect to the control variables p_{E_i} and m_{E_i}. In fact, when using a system of multiple coils, these can be all orientated towards the center of the workspace and a linear relationship between the current and generated field can be obtained - within a "small-enough" area of the workspace. In our case, these simplifications do not apply and deeper analysis is required.

To investigate the actuation capabilities of multiple EPMs, along the lines of [25], [24], we define the differential of the wrench as

$$
\begin{aligned}
\delta w_{ij} &= \begin{pmatrix} \frac{\partial w_{ij}}{\partial p_{ij}} & \frac{\partial w_{ij}}{\partial \hat{m}_{I_j}} \end{pmatrix} \begin{pmatrix} \delta p_{I_j} \\ \delta \hat{m}_{I_j} \end{pmatrix} + \begin{pmatrix} \frac{\partial w_{ij}}{\partial p_{ij}} & \frac{\partial w_{ij}}{\partial \hat{m}_{E_i}} \end{pmatrix} \begin{pmatrix} \delta p_{E_i} \\ \delta \hat{m}_{E_i} \end{pmatrix} \\
&\quad + \sum_{\substack{k=1 \\ k\neq j}}^{N} \begin{pmatrix} \frac{\partial w_{ij}}{\partial d_{jk}} & \frac{\partial w_{ij}}{\partial \hat{m}_{I_k}} \end{pmatrix} \begin{pmatrix} \delta p_{I_k} \\ \delta \hat{m}_{I_k} \end{pmatrix} \\
&= \begin{pmatrix} \frac{\partial w_{ij}}{\partial p_{ij}} & \frac{\partial w_{ij}}{\partial \hat{m}_{I_j}} \end{pmatrix} \begin{pmatrix} I & 0_{3,3} \\ 0_{3,3} & (\hat{m}_{I_j})_\times^T \end{pmatrix} \delta x_j \\
&\quad + \begin{pmatrix} \frac{\partial w_{ij}}{\partial p_{ij}} & \frac{\partial w_{ij}}{\partial \hat{m}_{E_i}} \end{pmatrix} \begin{pmatrix} I & 0_{3,3} \\ 0_{3,3} & (\hat{m}_{E_i})_\times^T \end{pmatrix} \delta q_i \\
&\quad + \sum_{\substack{k=1 \\ k\neq j}}^{N} \begin{pmatrix} \frac{\partial w_{ij}}{\partial d_{jk}} & \frac{\partial w_{ij}}{\partial \hat{m}_{I_k}} \end{pmatrix} \begin{pmatrix} I & 0_{3,3} \\ 0_{3,3} & (\hat{m}_{I_k})_\times^T \end{pmatrix} \delta x_k \\
&= J_{x_{ij}}\delta x + J_{q_{ij}}\delta q_i, \qquad (2)
\end{aligned}
$$

with $0_{k,l} \in \mathbb{R}^{k\times l}$ *zero matrix*, $(\cdot)_\times : \mathbb{R}^3 \to \mathfrak{so}(3)$ is the *skew operator* and $x = \begin{pmatrix} x_1^T & x_2^T & \dots & x_N^T \end{pmatrix}^T$. We refer to $x_j \in \mathbb{R}^6$, $j = 1, 2, \cdots, N$ as the representation of the j-th IPM pose (i.e. position and Euler angles) and to q_j as the representation of the j-th EPM pose.

We will focus on the manipulation of multiple DOFs in a point $p_I = p_{I_k} = p_{I_l}\ \forall\ i, l$, that does not vary with time, i.e. $\delta p_{I_j} = \delta m_{I_j} = 0\ \forall\ j$. We consider this scenario for two reasons: first, our aim is to focus on the manipulability properties in a fixed point within the workspace, with no constraints on the specific target point. Secondly, having multiple IPMs at the same point within the workspace represents the worst case scenario. In fact, the further the IPMs are apart, the more they behave as independent magnets (5 DOFs each). Moreover, under these assumptions, the interaction between IPMs can be neglected, which does not change the number of DOFs, when the wrench is fully controllable from the input $q = \begin{pmatrix} q_1^T & q_2^T & \cdots & q_M^T \end{pmatrix}^T$ [28]. This is discussed in the

next section.

The variation of wrench can thus be directly related to EPMs motion (or actuation) only, as

$$\delta w = J_q \delta q, \tag{3}$$

where $[J_q]_{ij} = J_{q_{ij}} \in \mathbb{R}^{6\times 6}$ is the i,j block of J_q and

$$w = \begin{pmatrix} \sum_{i=1}^{M} w_{1i} \\ \sum_{i=1}^{M} w_{2i} \\ \vdots \\ \sum_{i=1}^{M} w_{Ni} \end{pmatrix}.$$

III. Definition of Magnetic Manipulability

We intend (magnetic) *manipulability* to be the measure of the number of (magnetic) DOFs that can be (magnetically) manipulated by a (magnetic) actuation system. This means that, given a set of inputs (q), we aim to measure the number of variables (w) that can be independently actuated.

In the following, we prove that with 2 EPMs ($M = 2$) we can control 8 DOFs of 2 orthogonal IPMs ($N = 2$) in the same point of the worskspace. First, we need to prove that the magnetic DOFs of 2 orthogonal IPMs are 8 in the same point in space, as in [21]. This is straightforward since, in the same point, they experience the same magnetic field (B) and magnetic field jacobian $\left(\mathrm{d}B = \frac{\partial B}{\partial p}\right)$. Therefore,

$$\begin{aligned} w_{ij} &= \begin{pmatrix} \mathrm{d}B \; m_{I_j} \\ (m_{I_j})_\times B \end{pmatrix} \\ &= \left(\begin{array}{cccc|c} m_{I_{j_1}} & m_{I_{j_2}} & m_{I_{j_3}} & 0 & 0 & \\ 0 & m_{I_{j_1}} & 0 & m_{I_{j_2}} & m_{I_{j_3}} & 0_{3,3} \\ -m_{I_{j_3}} & 0 & m_{I_{j_1}} & -m_{I_{j_3}} & m_{I_{j_2}} & \\ \hline & & 0_{3,5} & & & \left|(m_{I_j})_\times\right. \end{array}\right) \begin{pmatrix} \frac{\partial B_1}{\partial e_1} \\ \frac{\partial B_1}{\partial e_2} \\ \frac{\partial B_1}{\partial e_3} \\ \frac{\partial B_2}{\partial e_2} \\ \frac{\partial B_2}{\partial e_3} \\ B \end{pmatrix} \\ &= S_j U. \end{aligned} \tag{4}$$

Here, $e_i \in \mathbb{R}^3$ is the i-th element of the orthonormal basis of $\mathbb{R}^3$.

Intrinsically, U depends on the pose of all the EPMs involved. We can write the relationship in (4) as

$$w = SU, \tag{5}$$

and (3), being m_{I_j} assumed constant $\forall j$, as

$$\delta w = S\frac{\partial U}{\partial q}\delta q = J_q \delta q,$$

with $S = \begin{pmatrix} S_1^T & S_2^T & \cdots & S_N^T \end{pmatrix}^T$. Therefore, $S\frac{\partial U}{\partial q} \equiv J_q$ and, as standard approach in robotics [29], the number of DOFs controllable from δq is $\mathrm{rank}\,(J_q)$.

Since $\mathrm{rank}\left(S\frac{\partial U}{\partial q}\right) \leq \min\left(\mathrm{rank}\,(S), \mathrm{rank}\left(\frac{\partial U}{\partial q}\right)\right)$ and $\mathrm{rank}\,(S) \leq 8$, the maximum number of DOFs we can control in a point is 8. It is known that, for any j, $\mathrm{rank}\,(S_j) = 5$. Moreover, one can notice that $\mathrm{rank}\,(S) = 8$, if $S = \begin{pmatrix} S_1^T & S_2^T \end{pmatrix}^T$ and $m_{I_1} \times m_{I_2} \neq 0$ (i.e. 2 IPMs are not parallel). Specifically, maximum manipulability is obtained with 2 orthogonal IPMs.

We can assume, from here on, that we select the two IPMs to be orthogonal and, thus, $\mathrm{rank}\,(S) = 8$. In this case,

$$\mathrm{rank}\left(S\frac{\partial U}{\partial q}\right) = \mathrm{rank}\left(\frac{\partial U}{\partial q}\right) = \mathrm{rank}(J_q),$$

thus, independently of the IPMs, we can investigate magnetic manipulability by analysing J_q or, equivalently $\frac{\partial U}{\partial q}$. However, the analysis of these matrices has two main disadvantages: they are nonlinear with respect to the control variables (q) and they map variations in the input (δq) onto the output (δw). Therefore, any solution is local and difficult to quantify. For this reason, we describe a more suitable approach to identify the DOFs, in the next section.

In a real scenario, we cannot guarantee the IPMs to be always orthogonal, when organized in a serial structure such as a continuum robot. This means that manipulability, as for general robotic systems [29], is a local property and there exist conditions of singularity. This can be physically avoided by mechanical constraints or considered in the controller design. For the scope of the presented work, we analyse IPMs in a non-singular scenario; avoiding dependence on their local configurations. However, we expect that there will exist situations for which some degree of controllability may be lost, in real applications.

IV. Degrees of Freedom Analysis

In the following, we will be considering the actuation of $N = 2$ *orthogonal* IPMs with $M = 2$ *independently actuated* EPMs. Increasing the number of EPMs would not have a real effect on the number of DOFs we can control in a point, due to the properties of the magnetic field: $\mathrm{rank}\,(S) \leq 8$ (see previous section).

Finding 8 independent DOFs is equivalent to finding 8 poses of the EPMs that led to 8 orthogonal directions of the wrench w onto the IPMs. This can be expressed as searching for the set $Q = \{q(T),\ T = 1,\ 2,\ \ldots,\ 8\}$ such that

$$\mathrm{rank}\,(w(1)\ \cdots\ w(8)) = \mathrm{rank}\,(S\,(U(1)\ \cdots\ U(8))) = 8.$$

Since, in this case, $\mathrm{rank}\,(S) = 8$,

$$\mathrm{rank}\,(S\,(U(1)\ \cdots\ U(8))) = \mathrm{rank}\,(U(1)\ \cdots\ U(8)).$$

Thus, we need to find 8 poses for which we obtain 8 independent $U(T),\ T = 1,\ 2, \ldots,\ 8$. Due to the nonlinearities of the problem, solving (4) or (1) with respect to q is not trivial. Therefore, we opted for a direct analysis of primitive poses, in terms of effects on the magnetic field, as detailed below. Some of the analysed poses are known to be suboptimal, due to the workspace limitations of the actuating robotic system: 2 LBR iiwa 14 (KUKA, Germany). However, they show independent activation of each field component. These poses are reported in Fig. 2 and their effect on the wrench applied to 2 orthogonal IPMs reported in Fig. 3. Specifically, in Fig. 3, we show the force and torque that are activated for each case of Fig. 2. To underline the independent DOFs activation, we schematically

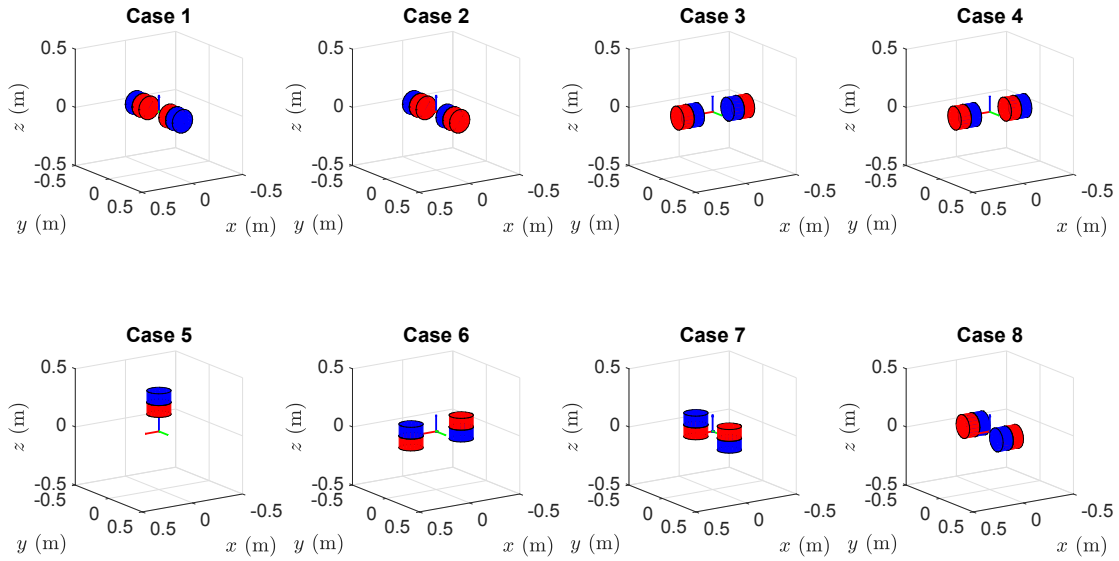

Fig. 2. EPMs poses for independent DOFs control; cases are shown with EPM-IPM center to centrer distance of 0.25 m.

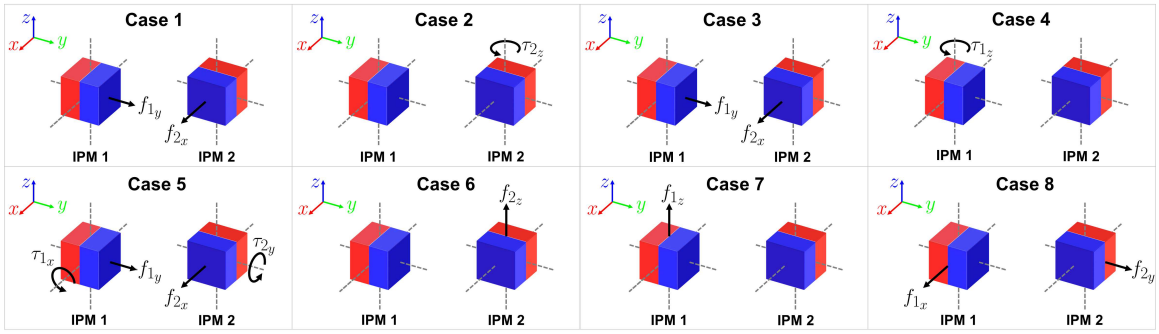

Fig. 3. Example of orthogonal IPMs and directions of the wrench applied for each of the cases of Fig. 2.

represent the components of field and differentials in Table I, according to the dipole model. These represent the directions of the 8 linearly independent vectors that led to the analysed DOFs. In particular, we normalized each component to its maximum value over the 8 cases and obtain the reported scale-free values. This eliminates any dependency between field and differentials strength, EPM-IPM distance and their respective size, and permits comparison between magnetic field and differentials, which are inherently different physical quantities. The strength of the actuation, being case-specific, could be changed by designing the geometric parameters of the magnets or controlled through EPM-IPM distance.

Poses for Field Solutions: The last 3 components of U (see (4)) are related to the magnetic field B. In order to have 3 orthogonal vectors $U(T)$, for different times T, we look for configurations where the magnets are aligned (case 2, 4, 5 in Fig. 2). In this case, by aligning the EPMs with each of the main axis, we obtain $\hat{B}(2) = e_2$, $\hat{B}(4) = e_1$ and $\hat{B}(5) = e_3$, thus 3 independent components of U. Due to physical limitations of the robots' workspace, reaching the bottom of the IPMs was not possible. Therefore, we propose the control of $U(5)$ by only using one EPM. This, inherently, generates differential components.

Poses for Differentials Solutions: To obtain independent components of U related to the differentials of the field, we consider solutions with no field components. This is achieved by positioning the EPMs in opposite directions (case 1, 3, 6, 7, 8). In both cases 1 and 3, we obtain differentials $\frac{\partial B_1}{\partial e_1}$ and $\frac{\partial B_2}{\partial e_2}$. In the cases 6, 7, 8, we obtain only the component $\frac{\partial B_1}{\partial e_3}$, $\frac{\partial B_2}{\partial e_3}$ and $\frac{\partial B_1}{\partial e_2}$, respectively.

V. Experimental Analysis

Validation of the proposed inferences, was performed through a series of experiments, aimed at proving the 8 DOFs manipulation capabilities. In particular, we tested 8 configurations of the EPMs for which we can control, independently, the 8 components of the field U, defined in

TABLE I

FIELD AND DIFFERENTIAL COMPONENTS IN THE 8 CASES, NORMALIZED TO THEIR MAXIMUM VALUE.

	Case 1	**Case 2**	**Case 3**	**Case 4**	**Case 5**	**Case 6**	**Case 7**	**Case 8**
$\frac{\partial B_1}{\partial e_1}$	$\frac{1}{2}$		-1		$\frac{1}{4}$			
$\frac{\partial B_1}{\partial e_2}$								1
$\frac{\partial B_1}{\partial e_3}$						1		
$\frac{\partial B_2}{\partial e_2}$	-1		$\frac{1}{2}$		$\frac{1}{4}$			
$\frac{\partial B_2}{\partial e_3}$							1	
B_1				1				
B_2		1						
B_3					1			

Section III. This proves the results in previous section, as reported in Table I.

Each experiment was performed by placing a 6-axis load cell (Nano17 Titanium, ATI, USA) between 2 robotic arms (LBR iiwa 14, KUKA, Germany); each manipulating one of the actuating EPMs (Cylindrical permanent magnet with a diameter and length of 101.6 mm and an axial magnetization of 970.1 Am^2 (N52)), as shown in Fig. 4. Each experiment was repeated twice, in order to emulate the presence of more than 5 DOFs in the same point of the workspace. To realize this arrangement experimentally, we captured the load cell data during EPMs manipulation first with an IPM (Cubic permanent magnet with length of 12.6 mm and an axial magnetization of 2.1 Am^2 (N42)) mounted along the global y axis (Config. 1, Fig. 4), and subsequently rotated the IPM to align with the x axis (Config. 2, Fig. 4) and repeated the EPMs manipulation sequence, detailed in Fig. 2.

For each of the *cases* reported in Fig. 2 and Table I, we performed an independent experiment, in order to better visualize the behaviour of the field[1], specifically, in its steady final configuration. The two robotic arms were controlled to the each pose reported in Fig. 2, synchronously, from an initial *zero-field pose*. This initial pose was found as a trade-off between reachable workspace, i.e. the one each end-pose would be reached from, and minimum field strength; to eliminate residual magnetic coupling, the load cell was de-biased in this initial configuration. A detailed video of the performed experiments can be found in media attached to the paper.

A total of 16 experiments were performed with the 8 cases being repeated twice (for each IPM orientation). The wrench $w_1(T)$ and $w_2(T)$ was measured on each load cell for every period $T \in [0, t_i]$, for the i-th case; note that $t_i \neq t_j,\ i \neq j$, in general, since some configurations can be reached faster than others from the same initial pose. We rearrange $w(T) = \left(w_1^T(T)\ w_2^T(T)\right)^T$ and, according to (5), we map the measured wrench onto the independent field components $U(T) = S^{\dagger} w(T)$; with $\cdot^{\dagger}$ we intend the *Moore-Penrose pseudoinverse*.

Our main aim is proving that the 8 components of the field U can be manipulated independently and, in particular, we are interested in their direction. Moreover, the magnetic field and its differentials are inherently measured on different scales and the maximum field we can generate is higher than its gradient, at the same relative distance between EPM and IPM. Therefore, for each case, we found the mean value of the last 20 s (once convergence is achieved), and normalized each component of the field to its steady state maximum value, over the 8 cases. This data processing eliminates any dependency between measured data and specific IPMs-EPM distance and magnets dimensions, giving an idea of the capabilities of this manipulation approach from a more general perspective.

In Fig. 5 we report the dynamic evolution of the field amongst the 8 experiments, as the EPMs move from initial to final pose. Each case is a combination of the data from the 2 independently analysed IPMs configurations. The title of each case was highlighted with the color of the component(s) of the field we expect to be activated, according to the static scenario in Fig. 6. In particular, Fig. 6(a) shows the generated field from the dipole model in (1), given the relative EPMs-IPMs pose and normalized to their maximum value ($|\overline{U}_i|$). Fig. 6(b) maps the field components activated for each experimental case ($|\overline{\hat{U}}_i|$), i.e. the mean steady state value (last 20 s) in Fig. 5. For comparison between the theoretical and experimental field, the error $|E_{U_i}| = |\overline{U}_i| - |\overline{\hat{U}}_i|$, is reported in Fig. 6(c).

In achieving control of the desired DOFs, significant activation of other components of the field is evident in certain cases; specifically, case 3, 4, and 6. This occurs due to the nature of the planned trajectory from the initial *zero-field pose* to the case-specific end pose. Indeed, trajectories were selected to achieve path length minimization, rather than minimizing cross-activation.

Fig. 6(b) shows that we can control 8 independent DOFs and, in particular, the components predicted by the dipole model. Through comparison of the measured and predicted values, less activation of U_1 and more activation of U_4 is apparent for case 1 and case 3, respectively. This is mainly due to the sensitivity of the gradient to accurate alignment between EPMs and IPMs, which is difficult to achieve open-loop.

From the absolute error $|E_U|$, reported in Fig. 6(c), we

[1]We refer to "field" as the vector field U, introduced in (4), to simplify the dissertation.

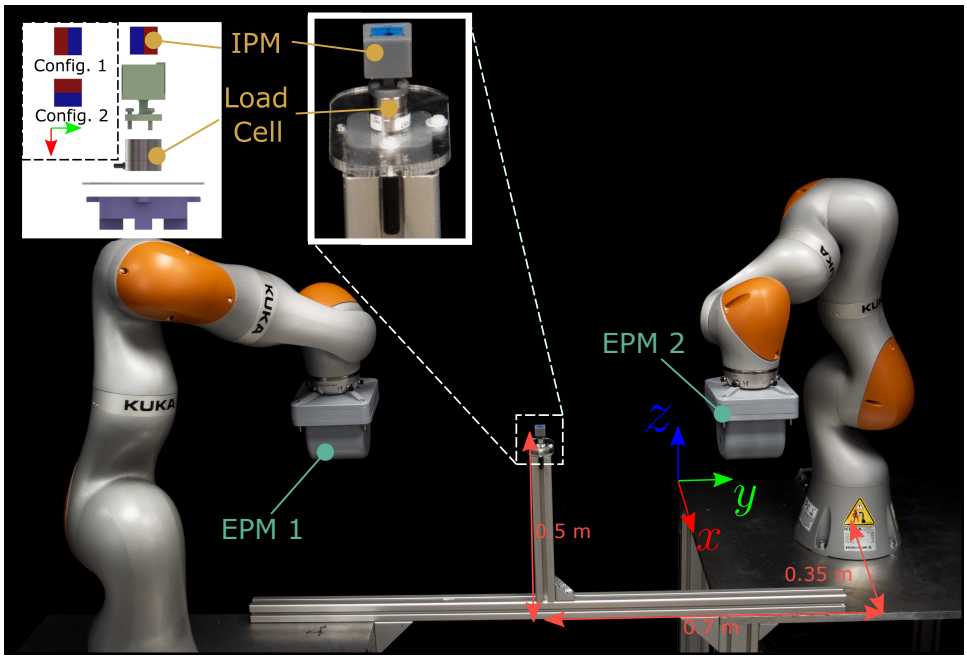

Fig. 4. Experimental Setup.

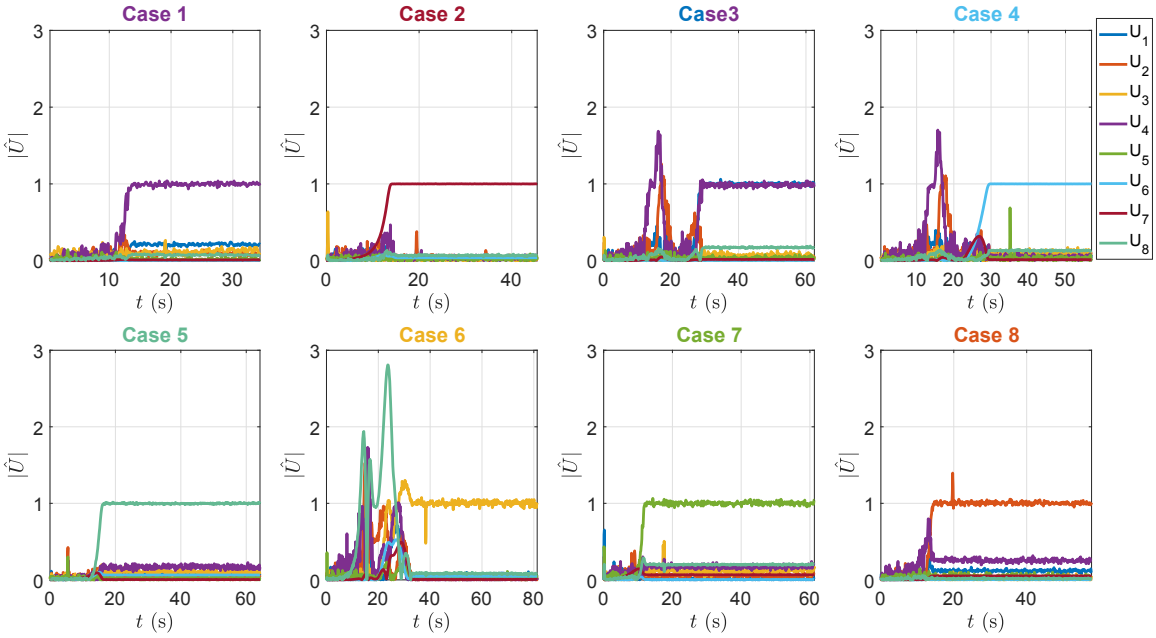

Fig. 5. Normalized response for magnetic field and differentials. Title colors are referred to the component activated for each case.

computed the mean percentage cross-activation

$$\overline{|E_U|}_{\%} = (5.4,\ 4.9,\ 7.9,\ 10.5,\ 2.5,\ 2.3,\ 2.4,\ 10.6)\,.$$

This was computed by considering only the components of E_U that are not desired to activate for each case, i.e. the blank boxes of Table I. This measures the cross-activation, intended as the amount of actuation in a direction that is not required to activate. This is the main difficulty in magnetic actuation: limiting the actuators to very fine control of specific DOFs, without cross-talk. In our case, by employing an open-loop dipole model-based method, we achieve 10.6% of cross-activation, in the worst case scenario. In practical application of the proposed actuation method, we will consider applying closed-loop wrench control [25], [24], which is expected to reduce these errors significantly.

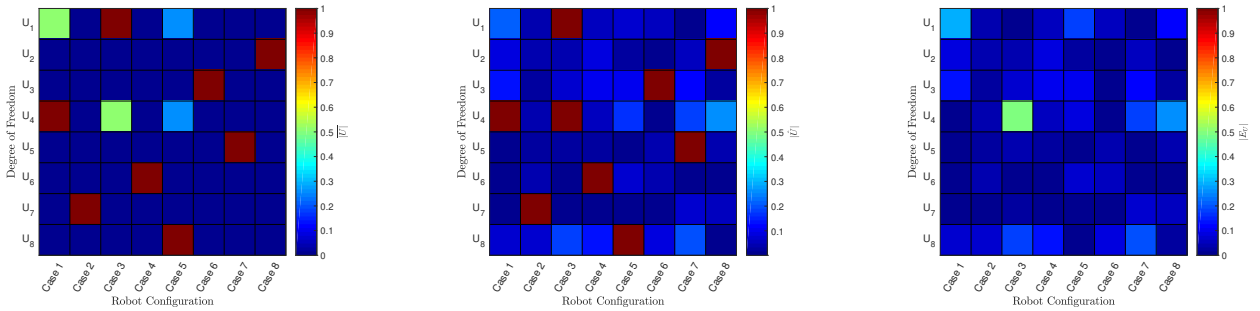

(a) Ideal. (b) Measured. (c) Error.

Fig. 6. Comparison of the ideal (dipole) U field generated by the poses in Fig. 2, as per Table I, and measured field, normalized to their maximum over the cases.

VI. Conclusions

The present work discussed the manipulation capabilities of robotically manipulated magnetic sources. In particular, we showed that 2 actuated EPMs are able to independently manipulate 8 DOFs.

Both theoretical dissertation and experiments prove that the proposed approach achieves same capabilities of coil based actuation [21], i.e. manipulation of 8 DOFs, in terms of wrench applied to 2 orthogonal independent IPMs within the workspace. The approach of using robotically controlled EPMs, compared to the usage of a coil-based counterpart, has the advantage of minimizing costs, energy consumption and maximizing the target workspace.

To improve the accuracy in controlling each component, future work will be focused on applying closed loop control of the wrench, as in [25], [24]. We expect that this approach would enhance the accuracy of control of single components, related EPM-IPM alignment, and reduce the errors related to dipole modeling.

Acknowledgment

The authors wish to thank Joseph C. Norton and Samwise Wilson for the help in designing the magnetic actuation system. We also thank Bruno Scaglioni and James W. Martin for facilitating our preliminary experiments.

References

[1] J. Burgner-Kahrs, D. C. Rucker, and H. Choset, "Continuum Robots for Medical Applications: A Survey," pp. 1261–1280, dec 2015.

[2] M. T. Chikhaoui and J. Burgner-Kahrs, "Control of Continuum Robots for Medical Applications : State of the Art," June 2018, pp. 25–27.

[3] M. Runciman, A. Darzi, and G. P. Mylonas, "Soft robotics in minimally invasive surgery," *Soft Robotics*, vol. 6, no. 4, pp. 423–443, 2019, pMID: 30920355. [Online]. Available: https://doi.org/10.1089/soro.2018.0136

[4] P. J. Swaney, J. Burgner, H. B. Gilbert, and R. J. Webster, "A flexure-based steerable needle: High curvature with reduced tissue damage," *IEEE Transactions on Biomedical Engineering*, vol. 60, no. 4, pp. 906–909, 2013.

[5] N. Simaan, K. Xu, W. Wei, A. Kapoor, P. Kazanzides, R. Taylor, and P. Flint, "Design and Integration of a Telerobotic System for Minimally Invasive Surgery of the Throat," *International Journal of Robotics Research*, vol. 28, no. 9, pp. 1134–1153, 2009.

[6] R. J. Webster, A. M. Okamura, and N. J. Cowan, "Toward active cannulas: Miniature snake-like surgical robots," in *IEEE International Conference on Intelligent Robots and Systems*, 2006, pp. 2857–2863.

[7] T. Kato, I. Okumura, H. Kose, K. Takagi, and N. Hata, "Tendon-driven continuum robot for neuroendoscopy: validation of extended kinematic mapping for hysteresis operation," *International Journal of Computer Assisted Radiology and Surgery*, vol. 11, no. 4, pp. 589–602, apr 2016.

[8] P. Breedveld, J. S. Sheltes, E. M. Blom, and J. E. I. Verheij, "A new, easily miniaturized steerable endoscope," *IEEE Engineering in Medicine and Biology Magazine*, vol. 24, no. 6, pp. 40–47, Nov 2005.

[9] G. Gerboni, P. W. J. Henselmans, E. A. Arkenbout, W. R. van Furth, and P. Breedveld, "HelixFlex : bioinspired maneuverable instrument for skull base surgery," *Bioinspiration & Biomimetics*, vol. 10, no. 6, p. 066013, dec 2015. [Online]. Available: https://doi.org/10.1088%2F1748-3190%2F10%2F6%2F066013

[10] N. Garbin, L. Wang, J. H. Chandler, K. L. Obstein, N. Simaan, and P. Valdastri, "Dual-continuum design approach for intuitive and low-cost upper gastrointestinal endoscopy," *IEEE Transactions on Biomedical Engineering*, vol. 66, no. 7, pp. 1963–1974, July 2019.

[11] S. Calò, J. H. Chandler, F. Campisano, K. L. Obstein, and P. Valdastri, "A compression valve for sanitary control of fluid driven actuators," *IEEE/ASME Transactions on Mechatronics*, pp. 1–1, 2019.

[12] J. Edelmann, A. J. Petruska, and B. J. Nelson, "Magnetic control of continuum devices," *International Journal of Robotics Research*, vol. 36, no. 1, pp. 68–85, 2017.

[13] S. Jeon, A. K. Hoshiar, K. Kim, S. Lee, E. Kim, S. Lee, J.-y. Kim, B. J. Nelson, H.-J. Cha, B.-J. Yi, and H. Choi, "A Magnetically Controlled Soft Microrobot Steering a Guidewire in a Three-Dimensional Phantom Vascular Network," *Soft Robotics*, vol. 6, no. 1, pp. 54–68, oct 2018. [Online]. Available: https://doi.org/10.1089/soro.2018.0019

[14] L. B. Kratchman, T. L. Bruns, J. J. Abbott, and R. J. Webster, "Guiding Elastic Rods With a Robot-Manipulated Magnet for Medical Applications," *IEEE Transactions on Robotics*, vol. 33, no. 1, pp. 227–233, 2017.

[15] J. Sikorski, I. Dawson, A. Denasi, E. E. G. Hekman, and S. Misra, "Introducing BigMag - A novel system for 3D magnetic actuation of flexible surgical manipulators," in *2017 IEEE International Conference on Robotics and Automation (ICRA)*, 2017, pp. 3594–3599.

[16] P. Valdastri, G. Ciuti, A. Verbeni, A. Menciassi, P. Dario, A. Arezzo, and M. Morino, "Magnetic air capsule robotic system: proof of concept of a novel approach for painless colonoscopy," *Surgical endoscopy*, vol. 26, no. 5, pp. 1238–1246, 2012.

[17] Y. Kim, G. A. Parada, S. Liu, and X. Zhao, "Ferromagnetic soft continuum robots," *Science Robotics*, vol. 4, no. 33, p. eaax7329, aug 2019. [Online]. Available: http://robotics.sciencemag.org/content/4/33/eaax7329.abstract

[18] A. Azizi, C. C. Tremblay, K. Gagné, and S. Martel, "Using the fringe field of a clinical MRI scanner enables robotic navigation of tethered instruments in deeper vascular regions," *Science Robotics*, vol. 4, no. 36, p. eaax7342, nov 2019. [Online]. Available: http://robotics.sciencemag.org/content/4/36/eaax7342.abstract

[19] O. Erin, H. B. Gilbert, A. F. Tabak, and M. Sitti, "Elevation and azimuth rotational actuation of an untethered millirobot by MRI gradient coils," *IEEE Transactions on Robotics*, vol. 35, no. 6, pp. 1323–1337, Dec 2019.

[20] X. Zhang, T.-A. Le, A. K. Hoshiar, and J. Yoon, "A Soft Magnetic Core can Enhance Navigation Performance of Magnetic Nanoparticles

in Targeted Drug Delivery," *IEEE/ASME Transactions on Mechatronics*, vol. 23, no. 4, pp. 1573–1584, 2018.

[21] S. Salmanipour and E. Diller, "Eight-Degrees-of-Freedom Remote Actuation of Small Magnetic Mechanisms," in *2018 IEEE International Conference on Robotics and Automation (ICRA)*, 2018, pp. 3608–3613.

[22] P. Ryan and E. Diller, "Magnetic actuation for full dexterity microrobotic control using rotating permanent magnets," *IEEE Transactions on Robotics*, vol. 33, no. 6, pp. 1398–1409, 2017.

[23] C. Heunis, J. Sikorski, and S. Misra, "Flexible Instruments for Endovascular Interventions: Improved Magnetic Steering, Actuation, and Image-Guided Surgical Instruments," *IEEE robotics & automation magazine*, vol. 25, no. 3, pp. 71–82, 2018.

[24] L. Barducci, G. Pittiglio, J. C. Norton, K. L. Obstein, and P. Valdastri, "Adaptive Dynamic Control for Magnetically Actuated Medical Robots," *IEEE Robotics and Automation Letters*, vol. 4, no. 4, pp. 3633–3640, jul 2019.

[25] G. Pittiglio, L. Barducci, J. W. Martin, J. C. Norton, C. A. Avizzano, K. L. Obstein, and P. Valdastri, "Magnetic Levitation for Soft-Tethered Capsule Colonoscopy Actuated With a Single Permanent Magnet: A Dynamic Control Approach," *IEEE Robotics and Automation Letters*, vol. 4, no. 2, pp. 1224–1231, 2019.

[26] J. J. Abbott, E. Diller, and A. J. Petruska, "Magnetic methods in robotics," *Annual Review of Control, Robotics, and Autonomous Systems*, vol. 3, no. 1, p. null, 2020. [Online]. Available: https://doi.org/10.1146/annurev-control-081219-082713

[27] A. J. Petruska and J. J. Abbott, "Optimal permanent-magnet geometries for dipole field approximation," *IEEE Transactions on Magnetics*, vol. 49, no. 2, pp. 811–819, 2013.

[28] A. Isidori, *Nonlinear control systems*. Springer Science & Business Media, 2013.

[29] B. Siciliano, L. Sciavicco, L. Villani, and G. Oriolo, *Robotics: Modelling, Planning and Control*. Springer Publishing Company, Incorporated, 2010.